Photoelectron angular distributions from multiphoton ionization of cesium atoms

R. N. Compton, J. A. D. Stockdale, and C. D. Cooper*
Chemical Physics Section, Health and Safety Research Division, Oak Ridge National Laboratory, Oak Ridge, Tennessee 37830

X. Tang and P. Lambropoulos
Department of Physics, University of Southern California, Los Angeles, California 90089-1341
(Received 29 June 1983; revised manuscript received 25 June 1984)

We present both experimental and theoretical studies of resonantly enhanced multiphoton ionization of cesium atoms. Photoelectron angular distributions for two-photon ionization via the one-photon-allowed $7p\ ^2P_{1/2,3/2}$ and $8p\ ^2P_{1/2,3/2}$ intermediate states and three-photon ionization via the two-photon-allowed $8d\ ^2D_{5/2,3/2}$ resonant intermediate states are reported. The photoelectrons are energy analyzed with a spherical-sector electrostatic energy analyzer with an energy resolution of ~ 0.1 eV and angular resolution of $\sim \pm 2°$. A straightforward calculation based upon a fine-structure scheme gives excellent agreement with the measured angular distributions for the $^2P_{1/2}$ states. The laser pulse duration is comparable to the hyperfine precession period which allows the hyperfine coupling to partially destroy the anisotropy initially produced in the $^2P_{3/2}$ resonant intermediate states. Quantitative calculations including hyperfine coupling take this into account and provide an expression which gives a reasonable fit to the $^2P_{3/2}$ data.

I. INTRODUCTION

The angular distributions of photoejected electrons provide valuable information about the structure of atoms and molecules and the photoionization process itself. The photoelectron angular distributions depend upon the nature of the initial bound state and final continuum states. The continuum contribution involves the interference between the partial waves of the outgoing electron, and any interaction between this electron and the ion core. The electron angular distribution resulting from the electric-dipole interaction between a single photon and an isotropic distribution of atoms is given by

$$\frac{d\sigma(\lambda,\Theta)}{d\Omega}=\frac{\sigma(\lambda)}{4\pi}[1+\beta P_2(\cos\Theta)]\ , \tag{1}$$

where σ is the total photoionization cross section at wavelength λ, $P_2(\cos\Theta)$ is the second Legendre polynomial, Θ is the angle between the polarization axis of the incident light and the direction of the photoelectron ($\vec{K}$), and β is the so-called asymmetry parameter.

In multiphoton ionization, the order of the process (i.e., number of photons involved) and the possible participation of real and virtual intermediate states are the two most important factors which determine the angular distribution. For the case of nonresonant multiphoton ionization or for resonantly enhanced multiphoton ionization and when the laser intensity is weak enough to validate the lowest order perturbation theory, the generalized cross sections for two- and three-photon ionization can be written as

$$\frac{d\sigma^{(2)}_{h\nu}(\lambda,\Theta)}{d\Omega}=\sigma^{(2)}_{h\nu}(\lambda)\frac{(1+\beta_2\cos^2\Theta+\beta_4\cos^4\Theta)}{4\pi\left[1+\frac{\beta_2}{3}+\frac{\beta_4}{5}\right]}\ , \tag{2}$$

$$\frac{d\sigma^{(3)}_{h\nu}(\lambda,\Theta)}{d\Omega}=\sigma^{(3)}_{h\nu}(\lambda)\times\frac{(1+\beta_2\cos^2\Theta+\beta_4\cos^4\Theta+\beta_6\cos^6\Theta)}{4\pi\left[1+\frac{\beta_2}{3}+\frac{\beta_4}{5}+\frac{\beta_6}{7}\right]}\ , \tag{3}$$

where the coefficients β_n are functions of microscopic atomic parameters and are independent of light intensity. The above expressions can also be written in terms of Legendre polynominals if it is deemed more convenient for data analysis.

A number of theoretical studies of angular distributions of photoelectrons from multiphoton ionization have been published.[1–5] Experimental measurements of angular distributions have been presented for two-photon ionization of sodium,[6,7] two-photon ionization of titanium,[8] two-photon ionization of cesium,[9] two- and three-photon ionization of strontium,[10] and five-photon (nonresonant) ionization of sodium.[11] The influence of nuclear spin on angular distributions has also been studied.[12] In addition, the effects of "quantum beats" due to the hyperfine levels on angular distributions have been observed.[13] Finally, angular distributions for so-called above threshold ionization of xenon at a fixed wavelength (0.53 μm) have been reported.[14] Both the experimental and theoretical studies have illustrated that measurements of angular distributions of photoelectrons from resonant multiphoton ionization are complicated by the following.

(i) The angular distributions may be laser power dependent due to saturation of some resonant level or due to ac Stark effects on the ground and excited states involved.[4]

(ii) So-called above threshold ionization[14,15] effects in which photoejected electrons gain energy from the radia-

tion field may complicate the measurements.

(iii) If more than one hyperfine level is excited (which is most often the case), quantum beat interference effects produce angular distributions which are dependent upon the temporal characteristics of the laser beam. For example, in two-photon ionization, the photoelectron angular distribution for the two-photon ionization of sodium via the $3^2P_{3/2}$ state is found to depend upon the time delay between the exciting and ionizing laser pulses.[13]

(iv) Sometimes subtle background or surface ionization effects are observed which can interfere with (or even obscure) the real signal (see, e.g., Ref. 7).

In this paper we present both theoretical and experimental studies of energy and angle resolved photoelectrons from two- and three-photon ionization of cesium atoms. Energy analysis of the photoelectrons is accomplished with a high resolution spherical sector electrostatic energy analyzer which circumvents many of the experimental problems described above. Quantitative comparison of theory and experiment shows the importance of hyperfine coupling in the $^2P_{3/2}$ intermediate state for the laser pulse durations used in these experiments and especially the experiments of Kaminski *et al.*[9]

II. EXPERIMENTAL

The experimental apparatus is shown in Fig. 1. A Molectron model uv-24 nitrogen laser ($\sim$1-MW peak power) was used to pump the oscillator and amplifier of a Molectron model DL-14 dye laser. The approximate laser power over the wavelength range used in these studies was 10 kW and the laser pulse duration was $\sim$10 ns. The laser is focused with a 35 mm lens. Using the manufacturer's quoted divergence of 2×10^{-3} radians for the dye laser and assuming that the focus is diffraction limited, one obtains an approximate power density at the focal volume of $\sim10^8$ W/cm^2. Neutral density filters were used to attenuate the laser power. Also, as the laser dye degraded, lower laser power was obtained. Angular distributions at all laser powers were identical. The bandwidth of the laser was $\sim$0.2 Å full width at half maximum (FWHM). A glan-air prism (Carl Lambrecht) was used to purify the linear polarization of the laser light and the polarization was rotated through a full 2π angle with one of two different Fresnel rhomb polarization rotators. Identical data were recorded with each rotator, and data obtained from π to 2π were identical with data recorded from 0 to π.

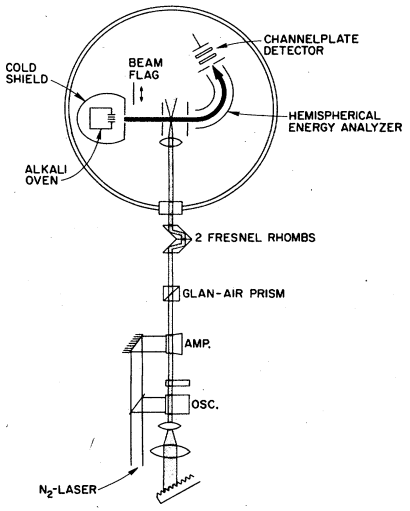

FIG. 1. Experimental arrangement for energy and angular distribution measurements for multiphoton ionization of alkali-metal atoms. The vacuum chamber is 3 ft in diameter and is pumped by a 6-in. oil diffusion pump with liquid nitrogen trap.

The cesium atom source consists of a stainless-steel hollow block with a multichannel hole array exit for producing a collimated cesium beam. A beam flag could be rotated in front of the beam. The alkali-metal beam crosses the laser focal volume through a small hole in a stainless-steel plate. The entire interaction volume is field free. Photoelectrons ejected 90° with respect to the propagation vector of the laser are energy analyzed by a spherical sector electrostatic energy analyzer.[16] Computer analysis of the ray traces through the analyzer indicates that the angular resolution of the analyzer was $\pm2°$. Energy analysis was accomplished by acceleration of the photoelectrons within the analyzer shield to an analysis energy of $\sim$5—10 eV. The theoretical resolution for this pass energy is 0.05 to 0.1 eV. The observed resolution was from 0.1 to 0.2 eV. The main factors which degrade resolution in multiphoton ionization experiments are (1) space-charge effects due to the large instantaneous signals produced, and (2) rf fields generated in space due to the firing of the laser. Both of these effects were minimized in the present experiment. Space-charge effects were minimized by lowering the alkali-metal beam intensity. When the ion density was too large, the electron energy distributions were broadened to lower energy. This is due to the fact that as the ion density builds up in time over the time length of the laser pulse, electrons are leaving from a higher and higher positive ion space charge. Thus, electrons are emitted at energies all the way from the expected energy $[3h\nu-V_{IP}(Cs)]$ to a lower energy cutoff corresponding to electrons leaving the fully developed positive ion cloud. By making the beam density and laser power large enough, it was possible to make this lower energy cutoff approximately zero. This means that those electrons created at the end of the laser pulse do not leave the positive ion cloud (plasma conditions). The Cs^+-ion energy distribution could also be studied by applying a small pusher voltage to accelerate the ions into the energy analyzer. As expected, the Cs^+ ion energy distribution extended to higher energy by the same amount that the electrons extended to lower energy. Further details of space-charge effects in multiphoton ionization will be published in a separate publication.[17] Certainly, the energy resolution was sufficient for the present purposes where only one electron energy was expected. Only one electron energy peak was observed under the typical operating conditions. At higher alkali-metal beam densities (source temperature) other low-energy electron peaks were observed which may be due to electron energy loss between the photoelectrons and *excited* alkali-metal atoms in the laser volume. Low-energy electrons are also expect-

ed from chemi-ionizing reactions between excited alkali-metal atoms and ground or excited atoms which produce ion pairs (e.g., $A_2^+ + e$ or $A^+ + A + e$). These reactions are not the subject of this paper.

The photoelectrons were detected with a dual channel-plate charged particle detector and the resulting signal was amplified and processed with a Princeton Applied Research boxcar averager. A 40-cm radius Helmholz coil was used to null the earth's field. This was imperative in order to operate the electron spectrometer at low pass energy.

III. THEORY

For relatively low-laser intensities, such as those employed in the present experiment, the photoelectron angular distributions can be cast in moderately simple forms exhibiting explicitly the atomic parameters on which they depend. Low intensity here implies that there is no significant core excitation and consequently a single-electron model is adequate. Saturation of the transition between the initial and the resonant interaction states would not affect the validity of the expressions as long as none of the ac Stark effects[5] associated with closely spaced intermediate resonances are important. All of the above conditions were certainly satisfied for all measurements reported in this work.

The general forms given in Eqs. (2) and (3) are obtained from the appropriate order of perturbation theory for an n-photon ionization process. The parameters β_n contain all the information pertaining to atomic structure and it is through the determination of such parameters that this information can be extracted from measurements of angular distributions. The ingredients of β_n are atomic matrix elements and phase shifts. We need not present derivations of the equations here as they can be found elsewhere.[5] Instead, we give a summary of the equations necessary for the interpretation of the experiments.

The final continuum state for the photoelectron is written as

$$f(r)\rangle = 4\pi \sum_{L=0}^{\infty} e^{-i\delta_L} G_L(\vec{K},\vec{r}) \times \sum_{M=-L}^{+L} Y^*_{LM}(\Theta,\Phi) Y_{LM}(\theta,\phi) , \quad (4a)$$

where $\vec{K}(\Theta,\Phi)$ is the wave vector of the outgoing photoelectron, $\vec{r}(r,\phi,\theta)$ is the position operator of the electron, G_L, the radial part of the continuum wave function depending parametrically on $\vec{K}$, and δ_L is the phase shift of the Lth partial wave. The sum over partial waves comes, of course, from the usual expansion of a continuum state in spherical harmonics. Since fine structure is resolved in the experiment the bound states are of the form $|n,m_j\rangle$ and spin is also included in the final state. In principle, there may be spin-orbit coupling in the continuum which may also make G_L dependent on j as well. The measurements reported herein would not detect such effects. For two-photon ionization, we have the initial $|6S_{1/2}\rangle$ state and the intermediate $|nP_{1/2}\rangle$ and $|nP_{3/2}\rangle$ states whose ionization by a second photon leads to $L=0$ and $L=2$ partial waves which interfere in the angular distribution. After the angular momentum algebra has been performed the resulting expression involves radial matrix elements between $6S_{1/2}$ and $6P_j$ and between $6P_j$ and the final state. In general, the radial parts of the wave functions for the bound states depend on j. This dependency is more pronounced for heavier elements. Let us denote by $R_D(j)$ the radial matrix element between $|nP_j\rangle$ and the $L=2$ partial wave, and by $R_S(j)$ the radial matrix element between $|nP_j\rangle$ and the $L=0$ partial wave of the final state. Since there is only one intermediate state involved in these resonant two-photon transitions, the bound-bound matrix elements cancel and the final result depends only on bound-free matrix elements. In fact, the angular distribution depends on the ratio of the two bound-free matrix elements. Thus, if we introduce the ratio $X = R_D(j)/R_S(j)$ we can write the angular distribution for the $P_{1/2}$ state as

$$\frac{d\sigma^{(2)}_{1/2}}{d\Omega} = 1 + \beta_2(1/2)\cos^2\Theta , \quad (4b)$$

where β_2 is given by

$$\beta_2(\tfrac{1}{2}) = \frac{3\chi^2 - 6\chi\cos(\delta_0-\delta_2)}{1+\chi^2+2\chi\cos(\delta_0-\delta_2)} . \quad (4c)$$

Without loss of generality, the microscopic parameter χ can be assumed to be real while δ_0, δ_2 are the total phase shifts for the S and D partial waves, respectively. As noted earlier, Θ is the angle between $\vec{K}$ and the direction of the polarization vector for linearly polarized light.

For the distribution through the $P_{3/2}$ state, we obtain

$$\frac{d\sigma^{(2)}_{3/2}(\Theta)}{d\Omega} = 1 + \beta_2(\tfrac{3}{2})\cos^2\Theta + \beta_4(\tfrac{3}{2})\cos^4\Theta , \quad (5a)$$

where

$$\beta_2(\tfrac{3}{2}) = \frac{3[5\chi^2+8\chi\cos(\delta_0-\delta_2)]}{4[1+\chi^2+2\chi\cos(\delta_0-\delta_2)]} \quad (5b)$$

and

$$\beta_4(\tfrac{3}{2}) = \frac{27\chi^2}{4[1+\chi^2+2\chi\cos(\delta_0-\delta_2)]} . \quad (5c)$$

The two independent parameters that can be determined from the experiment therefore are χ and $\delta_0-\delta_2$. If there is a significant dependence of wave functions or of phase shifts on j, it will be reflected in the parameters χ and $\delta_0-\delta_2$. The latter is expected to have by far the weakest dependence on j. The processes represented by the above equations can be viewed as ionization from an excited state except that in this case—with the exception of $P_{1/2}$—it is not an isotropically excited state because of the excitation with linearly polarized light.

The three-photon ionization angular distributions reported here involve a two-photon resonant excitation of either a $D_{3/2}$ or a $D_{5/2}$ state. The two-photon matrix elements leading from $6S_{1/2}$ to the D states involve summations over intermediate P states which were not resonant with the photon frequency. Since the transition is to a single resonant state the final expression again depends on the ratio of the two bound-free matrix elements; (in this

case the F and P partial waves) and the difference of the corresponding phase shifts.

For the process $6sS_{1/2}\rightarrow\rightarrow nD_{3/2}\rightarrow e^-$ the angular distribution is written as

$$\frac{d\sigma^{(3)}_{3/2}}{d\Omega}=1+\beta_2(\tfrac{3}{2})\cos^2\Theta+\beta_4(\tfrac{3}{2})\cos^4\Theta\ , \tag{6a}$$

where

$$\beta_2(\tfrac{3}{2})=\frac{7-18\chi^2-36\chi\cos(\delta_1-\delta_3)}{9[1+\chi^2+2\chi(\delta_1-\delta_3)]}\ , \tag{6b}$$

and

$$\beta_4(\tfrac{3}{2})=\frac{5[3\chi^2-2\chi\cos(\delta_1-\delta_3)]}{3[1+\chi^2+2\chi\cos(\delta_1-\delta_3)]}\ . \tag{6c}$$

The parameter χ is now defined as the ratio $R_F^{(j)}/R_P^{(j)}$ of the radial matrix elements for the F and P partial waves. For the process $6sS_{1/2}\rightarrow\rightarrow nD_{5/2}\rightarrow e^-$ and with the same definition for χ the angular distribution is

$$\frac{d\sigma^{(3)}_{5/2}(\Theta)}{d\Omega}=1+\beta_2(\tfrac{5}{2})\cos^2\Theta+\beta_4(\tfrac{5}{2})\cos^4\Theta+\beta_6(\tfrac{5}{2})\cos^6\Theta\ , \tag{7a}$$

where

$$\beta_2(\tfrac{5}{2})=\frac{12+37\chi^2+24\chi\cos(\delta_1-\delta_3)}{4[1+\chi^2+2\chi\cos(\delta_1-\delta_3)]}\ , \tag{7b}$$

$$\beta_4(\tfrac{5}{2})=\frac{5[13\chi^2+8\chi\cos(\delta_1-\delta_3)]}{2[1+\chi^2+2\chi\cos(\delta_1-\delta_3)]}\ , \tag{7c}$$

and

$$\beta_6(\tfrac{5}{2})=\frac{125\chi^2}{4[1+\chi^2+2\chi\cos(\delta_1-\delta_3)]}\ . \tag{7d}$$

All calculated distributions in this paper are based on the above equations with the parameters calculated using single-channel quantum defect theory with no allowance for any significant dependence on j of either the bound-free matrix elements or the phase shifts. It is, of course, known that the radial matrix elements between $6S_{1/2}$ and the nP_j states depend on j rather strongly with increasing n. This dependence would not affect the present experiments, however, because the matrix elements connecting bound states do not appear in the final expressions. The agreement with the experimental results seems to suggest that quantum-defect theory is adequate for the prediction of such experiments as long as it is assured that the collected electrons come from the excited state under consideration and not from other (especially molecular) channels. This is achieved here through the simultaneous electron energy analysis.

As discussed in the following section, some of the reported angular distributions may have been affected by hyperfine-structure (hfs) effects, while the theoretical expressions presented so far have been derived on the basis of a fine-structure (fs) scheme. Taking the transition $6S_{1/2}\rightarrow nP_j$ as an example, the fs picture implies that the first (linearly polarized) photon excites the $m_j=\pm\frac{1}{2}$ sublevels which are then ionized before the hyperfine coupling can destroy this anisotropy. For this condition to be satisfied either ionization must occur faster than the hfs precession period and/or the laser duration must be shorter than the hfs period. The latter is given by the inverse of the hfs splitting of the excited state. If neither of the above conditions is satisfied, the calculation must be performed in the hfs scheme.

Let us consider, as an example, the case of $7P_{3/2}$. The extreme hfs separation of the $F=2$ and $F=5$ levels is 198 MHz, while the laser duration is about 10 ns, which is comparable to the hfs period (5 ns). On the other hand, the laser intensity was not sufficiently large for ionization to occur faster than the hfs period. With the laser duration about equal to the hfs, we have a situation in which the results of the fs calculation may show a slight deviation from the experiment.

A calculation involving the hfs and an arbitrary laser pulse duration requires the complete time-dependent solution of the full density-matrix equations for all initial and intermediate states. In addition, knowledge of the detailed form of the laser pulse is required if the laser pulse duration is comparable to the hfs period, as is the case here. It is only in the limiting cases of very large or very short (compared to the hfs period) times that the detailed form of the laser pulse does not matter. An additional aspect that affects the theoretical interpretation is the degree of saturation of the bound-bound transition which requires rather accurate knowledge of the laser intensity. In view of these unknowns, we present here a somewhat simplified interpretation of the hyperfine effects which is adequate for the purposes of this paper.

We consider the set of the density-matrix equations from the hyperfine levels of $6S_{1/2}$ to all hyperfine levels of $7P_{3/2}$. Eliminating the off-diagonal matrix elements, we reduce the problem to a set of rate equations. The photoelectron angular distribution is then obtained from the ionization of the m_F sublevels of the F states into which the $7P_{3/2}$ is split. The calculation is lengthy and tedious. It will suffice to quote here the resulting expressions for the coefficients β_2 and β_4. They are now given by

$$\beta_2=\frac{3}{4}\frac{(9q-5)\chi^2-8\chi\cos\delta}{1+\chi^2+^2\chi\cos\delta}\ , \tag{8a}$$

$$\beta_4=\frac{27}{4}\frac{(1-q)\chi^2}{1+\chi^2+^2\chi\cos\delta}\ , \tag{8b}$$

where q is a parameter depending on angular momentum coefficients and the relative magnitudes of the laser duration and the hfs period. In the limit of very short laser pulses, q is zero. β_2 and β_4 then revert to the expressions (5b) and (5c) which are valid under pure fs conditions. In the limit of a very long laser pulse, q takes the value 0.7 which leads to an angular distribution resembling that of the level $7P_{1/2}$; it does not show a peak at $\pi/2$. This is to be expected since a long laser duration allows the hyperfine coupling to destroy the anisotropy created in the excitation of the nP state. Given that the pulse duration in this experiment is not controllable but still is of the order of the maximum hyperfine splitting of the $7P_{3/2}$, we ex-

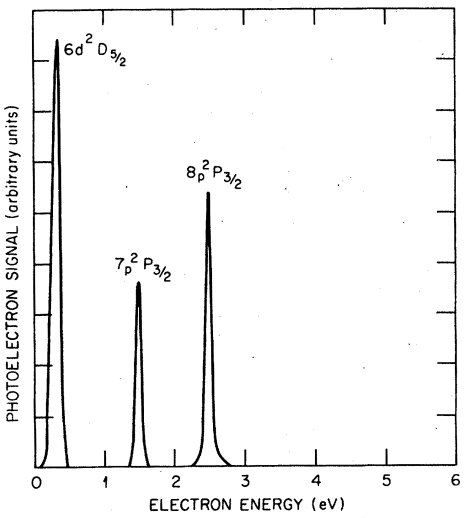

FIG. 2. Recorder traces of electron energy distributions for photoelectrons produced by multiphoton ionization of cesium. The energy scale was calibrated by fixing the $7p\ ^2P_{3/2}$ peak at its calculated energy position. The wavelength of the laser was tuned to one- or two-photon resonance with the states shown.

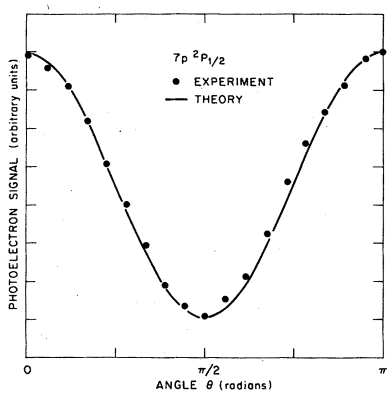

FIG. 3. Comparison of experimental and theoretical photoelectron angular distributions resulting from two-photon ionization of cesium atoms in which the first photon is in resonance with the $7p\ ^2P_{1/2}$ state. The experimental "error bars" in both intensity (photoelectron signal) and angle are approximately two times the size of a data point.

pect the data to be fitted best with coefficients β_2 and β_4 corresponding to a value of q between 0 and 0.7. The same expressions for β_2 and β_4 apply to the $8P_{3/2}$ state. Since its maximum hfs splitting is 91 MHz (about half that of $7P_{3/2}$) we expect the effect to be smaller and the appropriate value of q to be somewhat smaller. This is discussed further in the following section.

IV. RESULTS AND DISCUSSION

In Fig. 2 we show the electron energy spectrum for three of the resonant intermediate states reported in this study. No absolute energy scale was established, however, excellent self consistency among all of the peaks was observed. That is, by establishing an energy scale for one resonant intermediate level such as for the $7p\ ^2P_{3/2}$ state (which was done in Fig. 2), all other energy peaks correspond to the expected values [i.e., $2h\nu$-V_{IP}(Cs) or $3h\nu$-V_{IP}(Cs)]. Also an absolute energy scale could be established by using the known properties of the electrostatic energy analyzer and the voltage applied to the inner and outer spheres. Agreement on the energy of each peak was accurate to within ± 0.1 eV which is within the expected contact and surface potential differences.

The energy resolution at the peaks shown in Fig. 2 is 0.1 to 0.15 eV (FWHM) and was typical of the resolution obtained for the data presented in this paper. Resolution of 0.07 eV was obtained at lower pass energy through the analyzer. The entrance and exit apertures to the analyzer were 1 mm in diameter. Smaller apertures would also presumably afford better resolution. Resolution of 45 meV has been obtained in an identical analyzer by paying careful attention to space-charge effects, lower pass energies, and use of a laser with less rf noise.[18]

TABLE I. Calculated parameters used to determine the angular distributions of photoelectrons from multiphoton ionization of cesium. The β coefficients fit the equation $I(\Theta)=1+\beta_2\cos^2\Theta+\beta_4\cos^4\Theta+\beta_6\cos^6\Theta$.

	χ	δ_0	δ_2	δ_1	δ_3	β_2	β_4	β_6
$7P_{1/2}$	−2.35	11.66	4.46			6.56	0	0
$7P_{3/2}$	−2.35	11.70	4.47			−3.27	10.03	0
$8P_{1/2}$	−2.28	12.33	5.31			9.02	0	0
$8P_{3/2}$	−2.29	12.34	5.31			−3.33	12.35	0
$9P_{1/2}$	−2.23	12.47	5.55			10.74	0	0
$9P_{3/2}$	−2.23	12.47	5.55			−3.31	14.08	0
$10P_{1/2}$	−2.21	12.53	5.65			11.48	0	0
$10P_{3/2}$	−2.21	12.54	5.66			−3.29	14.80	0
$7D_{3/2}$	−5.72			7.75	−5.36	−1.88	7.51	0
$7D_{5/2}$	−4.46			7.76	−5.36	12.37	−43.00	46.88
$8D_{3/2}$	−4.56			8.39	−4.52	−1.79	8.84	0
$8D_{5/2}$	−4.12			8.39	−4.52	13.27	−46.03	51.39

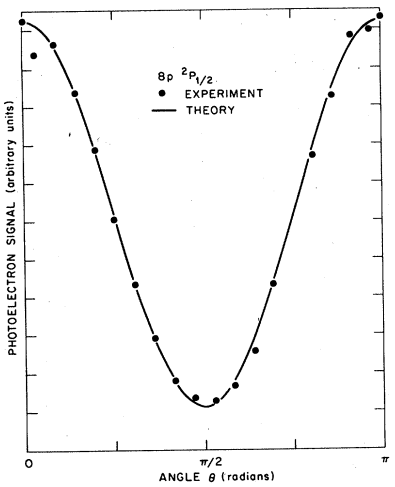

FIG. 4. Comparison of experimental and theoretical photoelectron angular distributions resulting from two-photon ionization of cesium atoms in which the first photon is in resonance with the $8p\ ^2P_{1/2}$ state. The experimental error bars in both intensity (photoelectron signal) and angle are approximately two times the size of a data point.

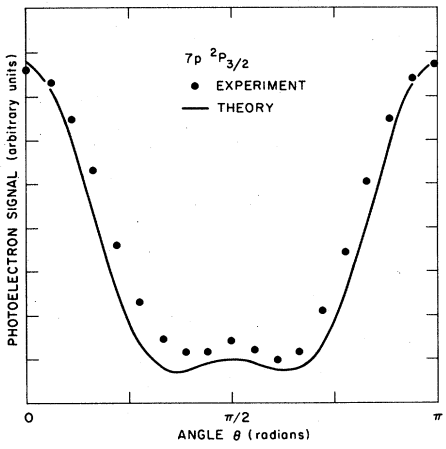

FIG. 5. Comparison of experimental and theoretical photoelectron angular distributions resulting from two-photon ionization of cesium atoms in which the first photon is in resonance with the $7p\ ^2P_{3/2}$ state. The experimental error bars in both intensity (photoelectron signal) and angle are approximately two times the size of a data point.

The calculated β parameters for resonantly enhanced two- and three-photon ionization of cesium atoms are presented in Table I. The β parameters completely determine the angular distributions as defined by Eqs. (2) and (3). Notice that a negative value for β_2 produces subsidiary peaks at $\Theta=\pi/2$. Calculations are also presented for two-photon ionization of cesium via the $9p\ ^2P_{3/2,1/2}$ and $10p\ ^2P_{3/2,1/2}$ states for which no experimental data are presented.

Figures 3 and 4 present both the experimental (solid points) and theoretical (solid lines) angular distributions for photoelectrons produced by linear polarized light for the $7p\ ^2P_{1/2}$ and $8p\ ^2P_{1/2}$ states, respectively. The estimated error associated with the experimental data points is assessed as twice the size of the actual data point on the graph. Taking into account this uncertainty, there is no discernible difference between theory and experiment. The experimental data was computer fitted to an Nth-order regression formula in powers of $\cos^2\Theta$. The best fit was obtained for an equation containing only the first order, i.e., $1+\beta_2\cos^2\Theta$. A comparison of the experimental and theoretical β values is shown in Table II. The experimental β_2 values for the $7p\ ^2P_{1/2}$ and $8p\ ^2P_{1/2}$ are 10% lower and $\sim$7% higher, respectively, than the theoretical values. No significance is attached to this difference. Theory seems to predict the experimental distributions very well.

Agreement between experiment and theory for the $7p\ ^2P_{3/2}$ and $8p\ ^2P_{3/2}$ distributions is poor as is seen in Figs. 5 and 6. The β_2 and β_4 values in Table II also illustrate this lack of agreement. The experimental measurements can be affected by hfs effects as discussed in Sec. III. As with any nitrogen laser pumped dye laser, the temporal profile of the laser pulse is not well defined. The nominal pulse width is 10 ns (FWHM) although intensity variations or "spikes" may occur within this time profile. Nevertheless, if we take $\sim$10 ns as the characteristic time for the excitation-ionization event we can consider the possible effects of the hfs. The hfs period for the $7p\ ^2P_{3/2}$ state is 5 ns which is on the order of the

TABLE II. Comparison of theoretical β values with those extracted from the experimental data. Experimental β values are determined from a computer fit of the third-order regression formula: $I(\Theta)=1+\beta_2\cos^2\Theta+\beta_4\cos^4\Theta+\beta_6\cos^6\Theta$.

	Theory			Experiment		
State	β_2	β_4	β_6	β_2	β_4	β_6
$7p\ ^2P_{1/2}$	6.56			5.95		
$7p\ ^2P_{3/2}$	−3.27	10.03		−0.55	6.32	
$8p\ ^2P_{1/2}$	9.02			9.62		
$8p\ ^2P_{3/2}$	−3.33	12.35		2.6	10.11	
$8d\ ^2D_{3/2}$	−1.79	8.84		0.38	5.13	
$8d\ ^2D_{5/2}$	13.27	−46.03	51.39	5.83	−18.2	21.52

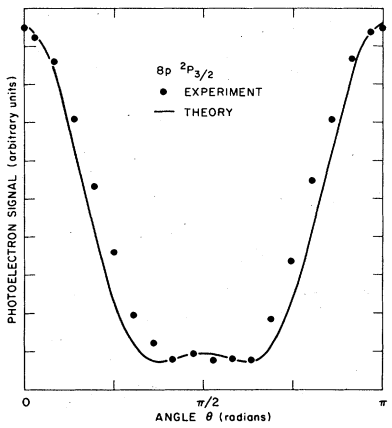

FIG. 6. Comparison of experimental and theoretical photoelectron angular distributions resulting from two-photon ionization of cesium atoms in which the first photon is in resonance with the $8p\ ^2P_{3/2}$ state. The experimental error bars in both intensity (photoelectron signal) and angle are approximately two times the size of a data point.

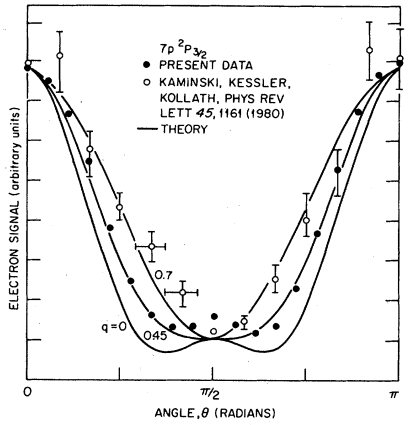

FIG. 7. Comparison of previous data [Kaminski, Kessler, and Kollath (Ref. 9)] with the present data. The experimental error bars in both intensity (photoelectron signal) and angle are approximately two times the size of a data point. The theoretical curves are calculated from the hyperfine structure β_2 and β_4 parameters given in Eqs. (8a) and (8b).

laser-pulse duration. Equations (8a) and (8b) give values for β_2 and β_4, respectively, as a function of the parameter q which depends upon angular momentum coefficients and the relative magnitudes of the laser duration of the hfs period. The other parameters in Eqs. (8a) and (8b) are given in Table III for the $7p\ ^2P_{3/2}$, and $8p\ ^2P_{3/2}$ states. q can vary from 0 (infinitely short laser pulse) to 0.7 (continuous laser pulse). Note that $q=0$ leads to the β_2 and β_4 value given in Table II. Figure 7 shows the present experimental data along with the earlier data of Kaminski *et al.*[9] and three calculations for $q=0$, 0.45, and 0.7. The data of Kaminski *et al.*[9] resembles a $1+\beta\cos^2\Theta$ distribution and is well fit by $q=0.7$. In this case, the long laser pulse allows for complete destruction of the orientation of $7p\ ^2P_{3/2}$ state. Equations (8a) and (8b) can be solved for q upon substitution of the experimental values for β_2, β_4, and $\cos\delta$ in Tables II and III. A q of ~ 0.3 satisfies both Eqs. (8a) and (8b). For $q=0.3$, β_2 is -0.32 and β_4 is 6.99. From Table II we see that the experimental value β_2 is -0.55 and β_4 is 6.32. The agreement is not perfect, however, inspection of Fig. 7 shows that the fit with experiment is greatly improved upon including the hyperfine effect.

A similar situation exists with respect to the $8p\ ^2P_{3/2}$ data. Here the hfs splitting is only 91 MHz and we expect the hyperfine effect to be smaller. Figure 8 shows the experimental data along with calculated distributions for $q=0$, 0.45, and 0.7. Again, the fit is not perfect in this case, and solving for q in the theoretical expressions [Eqs. (8a) and (8b)] using the experimental β_2 and β_4 values does not give a unique q value. Equation (8a) gives $q=0.5$ and Eq. (8b) gives $q=0.2$. The best fit to the data gives a q of about 0.3. Thus, a quantitative comparison of experiment and theory for the case of the $8p\ ^2P_{3/2}$ is not as satisfactory as for the case of the $7p\ ^2P_{3/2}$. However, visual inspection of Fig. 8 clearly shows that inclusion of the hyperfine effect improves the agreement between theory and experiment.

Photoelectron angular distributions for two-photon resonant three-photon ionization via the $8d\ ^2D_{3/2}$ state are shown in Fig. 9. The particular experimental data

TABLE III. Calculated parameters used to determine the hyperfine coupling effects upon the β_2 and β_4 values in Eqs. (8a) and (8b) for the $7p\ ^2P_{3/2}$ and $8p\ ^2P_{3/2}$ states.

State	χ	$\cos\delta$
$7p\ ^2P_{3/2}$	−2.354	0.594
$8p\ ^2P_{3/2}$	−2.2997	0.7390

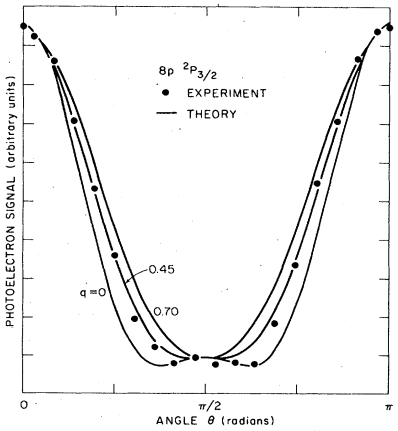

FIG. 8. Comparison of experimental and theoretical photoelectron angular distributions for two-photon ionization of cesium atoms in which the first photon is in resonance with the $8p\ ^2P_{3/2}$ state. The theoretical curves are calculated for three different values of hyperfine coupling parameters q [Eqs. (8a) and (8b)].

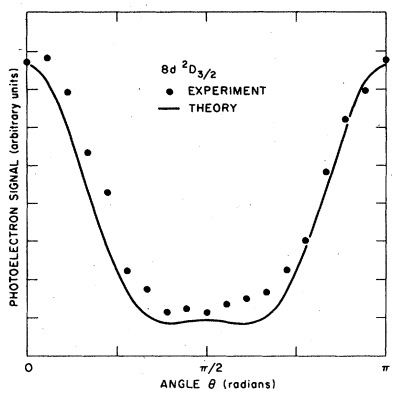

FIG. 9. Comparison of experimental and theoretical photoelectron angular distributions resulting from three-photon ionization of cesium atoms in which the second photon is in resonance with the $8d\,^2D_{3/2}$ state. The experimental error bars in both intensity (photoelectron signal) and angle are approximately two times the size of a data point.

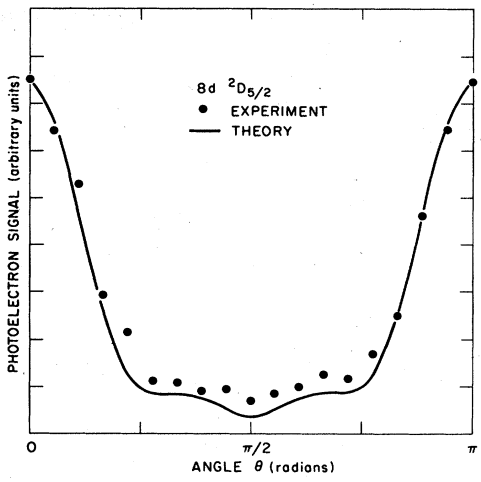

FIG. 10. Comparison of photoelectron angular distributions resulting from three-photon ionization of cesium atoms in which the second photon is in resonance with the $8d\,^2D_{5/2}$ state. The experimental error bars in both intensity (photoelectron signal) and angle are approximately four times the size of a data point.

presented in Fig. 9 do not show the subsidiary maximum at 90° predicted by theory. In some other experimental runs there was evidence for a maximum at 90°, however, the data shown in Fig. 8 is more representative of all the data. The subsidiary maxima at 90° for the $7p\,^2P_{3/2}$ and $8p\,^2P_{3/2}$ states were present in all of the angular distributions recorded. Angular distributions for the $8d\,^2D_{5/2}$ state are shown in Fig. 10. Three-photon ionization via the $8d\,^2D_{5/2}$ state requires terms up to $\cos^6\Theta$ in order to describe the process. Signal levels for the $8d$ states were not as large as those for the $7p$ or $8p$ states discussed above. As a result the error bars on the data points are assessed as approximately four times the size of a single point shown in the figures. The agreement with theoretical calculations again is not bad given the experimental uncertainty, however, the experimental data again lies slightly above the theory when normalized at $\Theta=0$ and π. The frequency splitting between the extreme hyperfine levels of the $8d\,^2D_{3/2}$ and the $8d\,^2D_{5/2}$ levels is 48 and 18 MHz, respectively. This corresponds to hyperfine periods of 20 ns ($8d\,^2D_{3/2}$) and 50 ns ($8d\,^2D_{5/2}$). Because of the short laser pulse and large photoionization cross section for d levels the hyperfine effect is not expected to have a large effect on the measured angular distributions. A detailed calculation was not performed on these levels so that quantitative comparison is not possible at this time.

V. CONCLUSIONS

We present a detailed comparison of experimental and theoretical photoelectron angular distributions for resonantly enhanced two- and three-photon ionization of an alkali-metal atom (cesium). In cases where the laser pulse duration is comparable to or larger than the hyperfine coupling period of the resonant intermediate state it is necessary to include hyperfine coupling effects in describing the angular distributions. It is also shown that the earlier results of Kaminski *et al.*[9] were likewise affected by mixing of the resonant hyperfine intermediate state.

ACKNOWLEDGMENTS

This research was sponsored by the Office of Health and Environmental Research, U.S. Department of Energy, under Contract No. W-7405-eng-26 with the Union Carbide Corporation. X.T. and P.L. acknowledge support by National Science Foundation Grant No. PHY-8100251.

*Department of Physics, University of Georgia, Athens, GA 30601.

[1]M. M. Lambropoulos and R. S. Berry, Phys. Rev. A **8**, 855 (1983).

[2]For reviews of various aspects of multiphoton ionization and photoelectron angular distributions see: P. Lambropoulos, in *Advances in Atomic and Molecular Physics* (Academic, New York, 1976), Vol. 12, pp. 87—164; *Multiphoton Processes*, edited by J. H. Eberly and P. Lambropoulos (Wiley, New York, 1978); J. Morellec, D. Normand, and G. Petite in *Advances in Atomic and Molecular Physics* (Academic, New York, 1982), Vol. 18, pp. 97—164.

[3]J. C. Tully, R. S. Berry, and B. J. Dalton, Phys. Rev. **176**, 95 (1968).

[4]S. D. Dixit and P. Lambropoulos, Phys. Rev. Lett. **46**, 1278 (1981).

[5]S. N. Dixit and P. Lambropoulos, Phys. Rev. A **27**, 168 (1983).
[6]J. S. Duncanson, Jr., M. P. Strand, A. Lindgrard, and R. S. Berry, Phys. Rev. Lett. **37**, 987 (1976).
[7]J. C. Hansen, J. A. Duncanson, Jr., R.-L. Chien, and R. S. Berry, Phys. Rev. A **21**, 222 (1980).
[8]S. Edelstein, M. M. Lambropoulos, and R. S. Berry, Phys. Rev. A **9**, 2459 (1974).
[9]H. Kaminski, J. Kessler, and K. J. Kollath, Phys. Rev. Lett. **45**, 1161 (1980).
[10]D. Feldmann and K. H. Welge, J. Phys. B **15**, 1651 (1982).
[11]G. Leuchs and S. J. Smith, J. Phys. B **15**, 1051 (1982).
[12]M. P. Strand, J. Hansen, R.-L. Chien, and R. S. Berry, Chem. Phys. Lett. **59**, 205 (1978); R.-L. Chien, O. C. Mullins, and R. S. Berry, Phys. Rev. **28**, 2078 (1983).
[13]G. Leuchs, S. J. Smith, E. Khawaja, and H. Walther, Opt. Commun. **31**, 313 (1979).
[14]F. Fabre, P. Agostini, G. Petite, and M. Clement, J. Phys. B **14**, L677 (1981).
[15]P. Agostini, F. Fabre, G. Mainfray, G. Petite, and N. K. Rahman, Phys. Rev. Lett. **42**, 1127 (1979).
[16]R. J. Warmack, J. A. Stockdale, and R. N. Compton, Int. J. Mass Spectrom. Ion Phys. **27**, 239 (1978).
[17]A. Dodhy, J. A. D. Stockdale, and R. N. Compton (unpublished).
[18]J. C. Miller and R. N. Compton. Chem. Phys. Lett. **93**, 453 (1982).